New Orleans JAZZED about Engineering Education

Paper ID #14484

Research Learning Experience while Designing Wind Turbine for Low Speed Wind Applications

Dr. Adeel Khalid, Kennesaw State University

Adeel Khalid, Ph.D. Associate Professor Systems Engineering Office: 678-915-7241

Mr. Christopher Douglas Roper, Kennesaw State University

Enrolled in a dual-degree program with the University of West Georgia and Kennesaw State University (formally Southern Polytechnic State University). Senior engineering student double majoring in physics and mechanical engineering with minors both in aerospace engineering and mathematics. Expertise both in the professional industry and with laboratory experience. Performed engineering and scientific applications under engineers and scientists as a materials intern, physics and engineering researcher/teacher's assistant, and mechanical engineer coop. Placed 2nd in the 2015 FRC Technical Research Exhibition Poster Presentation and 3rd in the 2015 FRC Technical Research Exhibition Oral Presentation in Region III for National Society of Black Engineers.

Research Learning Experience while Designing Wind Turbine for Low Speed Wind Applications

Abstract

Extracting the maximum amount of energy in various slow wind regions using low-speed wind turbines has provided challenges. The focus of this research project is to explore several factors to help analyze and distinguish the most efficient wind turbine blade designs. The researchers test the design the wind turbine blades by implementing two methods; Computational Fluid Dynamic analysis and 3-D printed prototype testing using Windlab laboratory apparatus. The data and analysis helps determine how to maximize the power extraction from wind energy. The value of undergraduate research experience is highlighted.

Keywords

Low speed wind turbine, blade design, Computational Fluid Dynamic analysis.

Introduction and Theory

Wind turbine energy methods and the usage of electrical power have been in practice for more than a century. Wind energy has been investigated heavily due in part to the detrimental environmental impacts of the use of fossil fuels and high price of fuel consumption. Scientists and engineers have developed numerous designs and modifications of many wind turbines. Typically wind farms are concentrated in the high-speed wind locations, and generally located in west mid-west of the United States. On the other hand, low speed wind occurrences – specifically in the eastern U.S. provides these regions an opportunity to complement the renewable energy for high demand energy consuming areas. Application of wind resources and its feasibility in Georgia are explored.

In low speed wind occurrences, wind travels at up to 9.1 mph, or 4.07 m/s^5. Low wind speeds can be harnessed to provide maximum extracted power from the Atlanta metropolitan city, county outskirts, and the coast of Savannah, Georgia. With careful consideration of the physical design of the wind turbine blade, improvements and modification in extracted power from low speed winds is possible. In this ongoing study, researchers explore low speed wind turbine designs, and experimentally test them for low speed environmental conditions using laboratory apparatus. Analysis from computational fluid dynamics demonstrates that variation of the twist angle and taper ratio result in a greater lift force coefficient with minimal drag force coefficient. To validate the computational fluid analysis, 3-D printed prototype of the most promising turbine blades are experimentally tested. A geometric baseline blade design is chosen to preform trial experiments. Two promising designs, with variations in taper ratio and blade twist angle, are carefully analyzed based on their parameter modifications. 3-D printed fabrication and wind tunnel experimentation is performed to compare the results with those obtained from the CFD analysis.

Literature Review

Wind turbine energy can be generated by two forms of energy, mechanical and electrical. Satpathy et al present a control strategy for the operation of a variable speed stand-alone wind turbine[7]. As wind travels in the pathway of the wind turbine, which consists of electrical generator, shaft and rotor blades, the blades will experience forces that cause them to overcome the inertia and then start extracting power from the free stream. Richardson et al discuss the development of the wind energy system and highlight the operating and design principles[8]. Sahin[9] also highlights the importance of wind energy and summarizes how this clean, practical, economical and environmentally friendly energy source has garnered renewed interest in this technology in the twenty first century. There are two types of blade designs frequently used, horizontal axis wind turbines (HAWTs) and vertical axis wind turbines (VAWTs); both systems have the potential to be aerodynamically optimized[2]. The blades are essentially based on the lift principle from aerodynamics, similar to the effects of an aircraft wing. Broe and Howell highlight the potential use of small wind turbines in horizontal and vertical axis configurations[11, 12]. Detailed CFD analyses have been performed in various studies conducted by Abdullah, Alessandro, Francesco et al[13-15]. Physics based models describe that an increase of a fluid flow, such as air, results in a decrease of pressure. With the wind turbine, the pressure below the blade will be greater than the air pressure above the blade, thus a lift force is generated[1]. The mechanical energy of the rotation of the blades generates torque to produce electrical energy within the system; this allows the electricity to be harnessed[8]. Wind tunnel testing and other experimental analyses have been conducted in studies performed by Treuren, Emejeamara and Dossena[16-18]. These studies have shown the efficacy and importance of wind turbines for small energy utilization environments.

The vertical wind turbines are used to optimize energy utilization. Slow wind speeds are optimal for a mini power generation systems. Various methods are investigated to achieve maximum efficiency from the wind turbine. Studies show that the changes in the geometric parameters of a wind turbine such as the number of blades, radius of blades, blade chord etc. can affect the amount of power extraction[2]. These parameters help determine how much of the energy from the wind can be extracted. Betz, determined theoretically and experimentally that the most energy that any device can extract is 59% of the total energy contained in the wind source[2].

Methodology

The National Renewable Energy Laboratory Phase VI wind turbine blade[3] is investigated for Computational Fluid Dynamic (CFD) validation study. The process consists of maximizing power production from the aerodynamic design of a winglet for a wind turbine blade. The study utilizes the computational fluid analysis tool. The NREL VI experiment conducted by Elfarral, Monier A., Nilay Sezer Uzol, and Sinan Akmandor[3] is replicated to help understand, demonstrate, as well as validate the researchers' findings. The parametric model consists of 19 sections with the structure of National Renewable Energy Laboratory cylindrical base section of the S809 airfoil. The validation for the NREL Phase VI CFD simulation is conducted using Solidworks. This software allows design, and development of windmill blades and computational fluid dynamic (CFD) analysis. In this case study, $5ms^{-1}$ wind speed is used since it replicates the wind conditions in the local regions of Georgia. In this research, final results show

a comparison of the validation study and the experimental analyses at $5ms^{-1}$. Figure 1 shows the final computer aided 3-D model of the designed NREL VI geometric blade for test comparison.

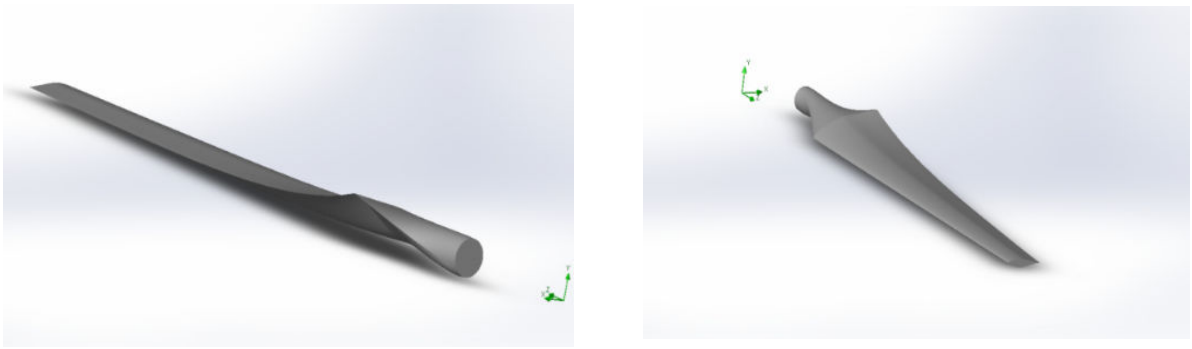

(a) (b)

Figure 1: NREL Phase VI 3D geometric blade design;

(a) Reverse isometric view of NREL CAD design. **(b)** Isometric view of NREL CAD design.

The validation comparison is made between Normal Force Coefficient C_N and the Non-dimensional Span at $5ms^{-1}$. Figure 2 shows the validator's experimental results that measure at 30%, 47%, 63%, 80%, and 95% span of the blade where the normal force coefficient can be displayed at each geometric section.

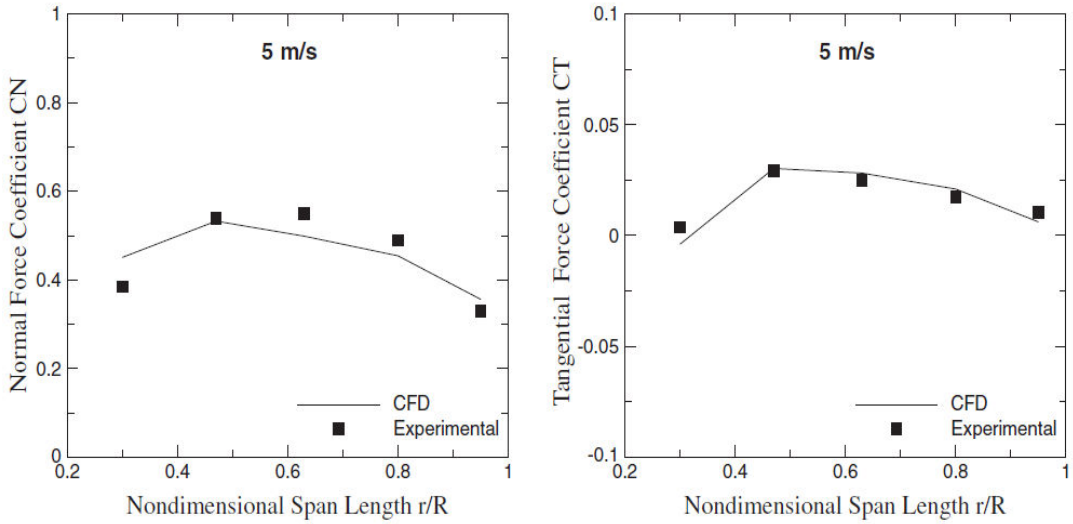

Figure 2: Normal Force Coefficient C_N versus the Non-dimensional Span at $5ms^{-1}$ from NREL VI Experiment[3]

The computational fluid analysis is conducted at the same experimental parameters and conditions as those used in the study performed by Elfarral, Monier A., Nilay Sezer Uzol, and Sinan Akmandor[3]. Non-dimensional normal force on the blades is calculated as a function of the

blade span and plotted for the CFD and experimental analyses and compared with the results obtained by Elfarra et al[3]. It can be observed that the results obtained from the validation study match closely with those of the published results. The process helps calibrate the CFD tool for further analyses as described in this paper.

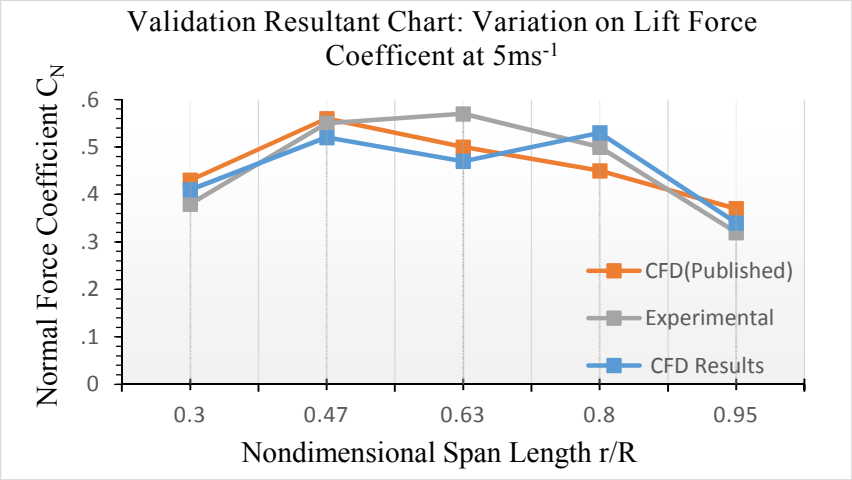

Figure 3: Normal Force Coefficient C_N versus the Non-dimensional Span at $5ms^{-1}$ validation study.

Design Specifications

The wind turbine blade selection that is enhanced and developed in this study is the Turbine Technologies blade model. The turbine blade model is instrumented and conducted in the Windlab apparatus shown in Figure 4.

(a) Windlab wind tunnel (b) Close up view on wind turbine rotor mechanism

Figure 4: Turbine Technologies Windlab Apparatus. *Courtesy of Turbine Technologies*

A baseline blade model is chosen. Incremental changes are made to the baseline by making modifications to each of the variables. The variables such as maximum chord, twist angle, taper ratio etc. are increased or decreased by 10%, 15%, 20% with respect to the initial baseline. The objective of varying the design parameters, shown in Table 1, is to explore and identify the most

efficient combination of design modifications for maximum power extraction at low speed wind conditions. A total of thirty models are created in order to explore the incremental changes of the wind turbine blades. One variable is changed at a time from the baseline parameters. For an example, starting with max chord, there are six modifications. These range between -20 and +20% of the baseline value with 5% increments and replace the original baseline value of the max chord. The rest of the parameters in the baseline column remain constant. This results in six different max chord modifications to the baseline. When this process is repeated for each row in the variables section, it results of 30 unique blade designs. Table 1 represents the variables that change due its modified parameters from the baseline design.

Table 1: Variable and parameter design specifications for Windlab Turbine Technologies Blade.

Variables	**Parameters**						
	20%	15%	10%	Baseline	-10%	-15%	-20%
Max. Chord (m)	0.115824	0.110998	0.106172	0.09652	0.086868	0.082042	0.077216
Twist Angle (degrees)	48.72	46.69	44.66	40.6	36.54	34.51	32.48
Taper Ratio	0.789468	0.7565735	0.723679	0.65789	0.592101	0.559206	0.526312
Angle of Incidences (degrees)	72.84	69.805	66.77	60.7	54.63	51.595	48.56
Number of Blades	3	3	3	3	3	2.55	3
Span (m)	0.50292	0.481965	0.46101	0.4191	0.37719	0.356235	0.33528

From the parameter and variable table, the designs are carefully studied and analyzed based on various factors. It is critical to test all designs in CFD analysis even if the theoretical predictions on some CAD models are not reasonable. For example, the +10, +15, +20 Span increase variations exceed the physical boundary of the Windlab wind tunnel apparatus during installation. With the baseline model complete, several modifications are made to the CAD model with respect to the variables and parameters chart shown in

Computational Analysis

The designed models are carefully studied and analyzed based on the data gathered from computational fluid analysis. The computer aided windmill blades are exposed to a wind velocity of 5 ms^{-1} in the horizontal x-directional plane. The lift and drag force equations are used to calculate the lift and drag coefficients. Lift force and drag forces are represented by Eq. (1) and Eq. (2) respectively:

$$L = \frac{1}{2} C_L A \rho V^2 \quad (1)$$

$$D = \frac{1}{2} C_D A \rho v V^2 \quad (2)$$

C_L is representing coefficient of lift force, C_D defining the coefficient of drag force, ρ depicting density of air, V representing the freestream velocity, A displaying the area for the body section. The lift and drag equations are programed into the Solidworks software to compute the aerodynamic parameter. The baseline of the fundamental design is the first to be experimentally tested using the computerized simulated wind tunnel. Final results are collected and plotted with respect to specific span sections of the turbine blade. Proceeding with all CAD models, each one is tested with the same parameters and constraints as the baseline model for consistency. With careful and detailed analysis, best designed characteristics are selected for further exploration and study.

As the span increases, the impact results in the coefficient of lift and drag decreasing linearly. The increase in span will cause the blade to gain more mass, resulting a greater force to overcome the inertial threshold rotation velocity. This will also cause the turbine blade to mimic a drag plate, thus increasing the coefficient of drag significantly. From the variations of span modifications, the +10% increase in span displays the most desirable lift and drag coefficient. As the taper ratio increases, the coefficient of lift increases. On the other hand, as the taper ratio decreases the coefficient of drag increases proportionally. The+10% and +20% increase in taper ratio theoretically provide the most promising results, yet the -20% taper ratio displays an average consistency from both drag and lift force coefficient overall.

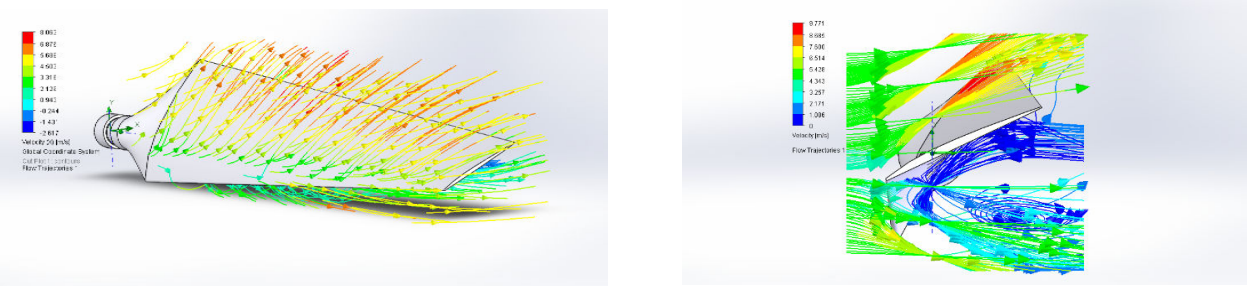

Figure 5: (a) Baseline wind analysis in geometric view. (b) Baseline wind CFD frontal analysis

Experimental Analysis

From the CFD simulation carried out through the experiment, values of coefficient of lift and drag force are obtained. These values from flow analysis are then separated as follows:

I. Effect of Angle of Incidence
II. Effect of Max Chord
III. Effect of Span
IV. Effect of Taper Ratio
V. Effect of Twist Angle

The graphs display all of the parameter modifications with respect to the baseline design. Modifications are made only to one parameter at a time, incrementally increasing from -20%, -15%, -10%, 10%, 15%, and 20%. Figures 6 through 10 show the force coefficients calculated using computational fluid analysis. These figures show the comparison of the various parameter changes with respect to the blade span at $5ms^{-1}$

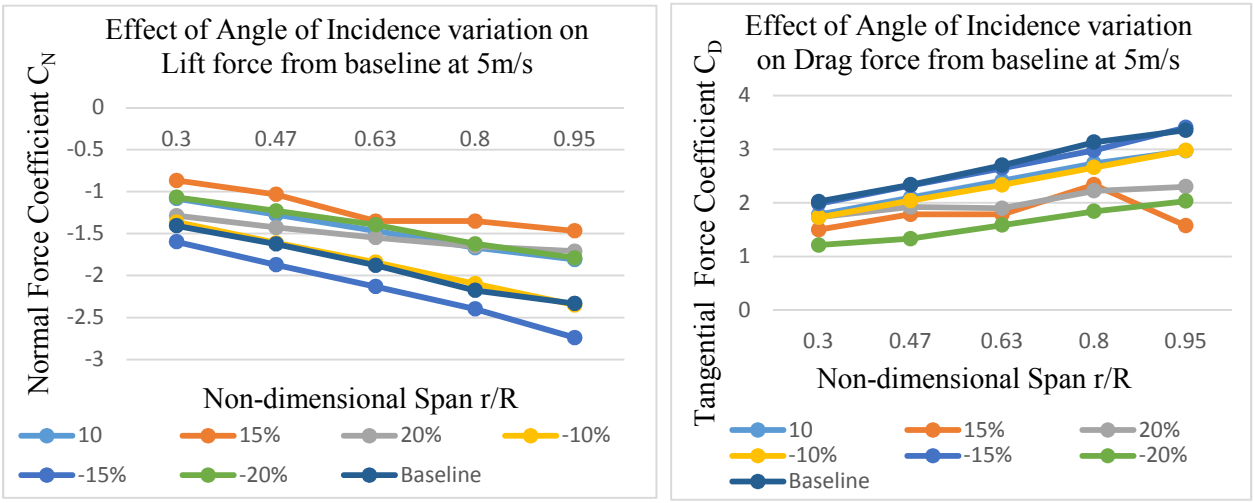

Figure 6: Normal force coefficient specification for Angle of Incidence at 5ms^{-1}

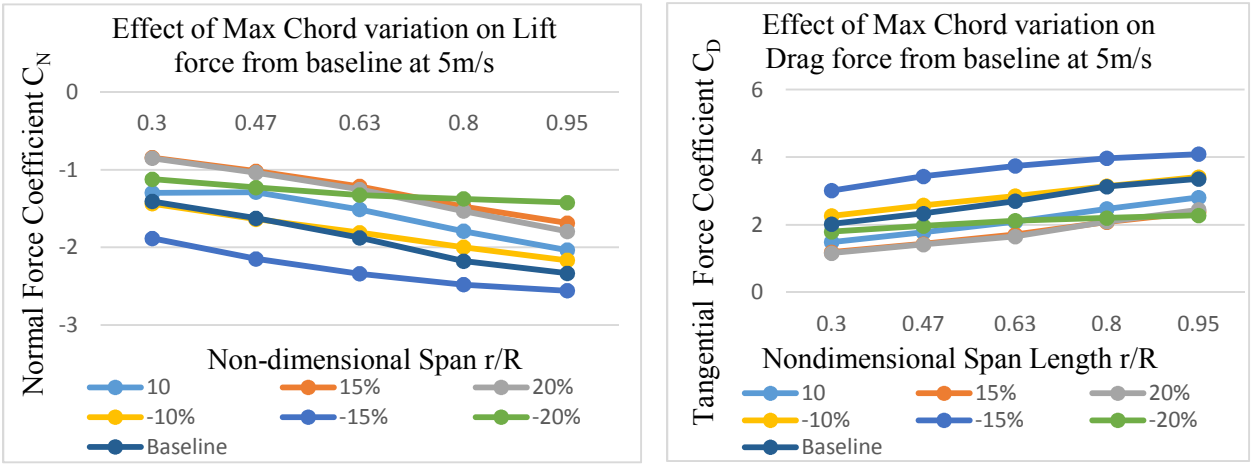

Figure 7: Normal and Tangential force coefficient specification for Max Chord at 5ms^{-1}

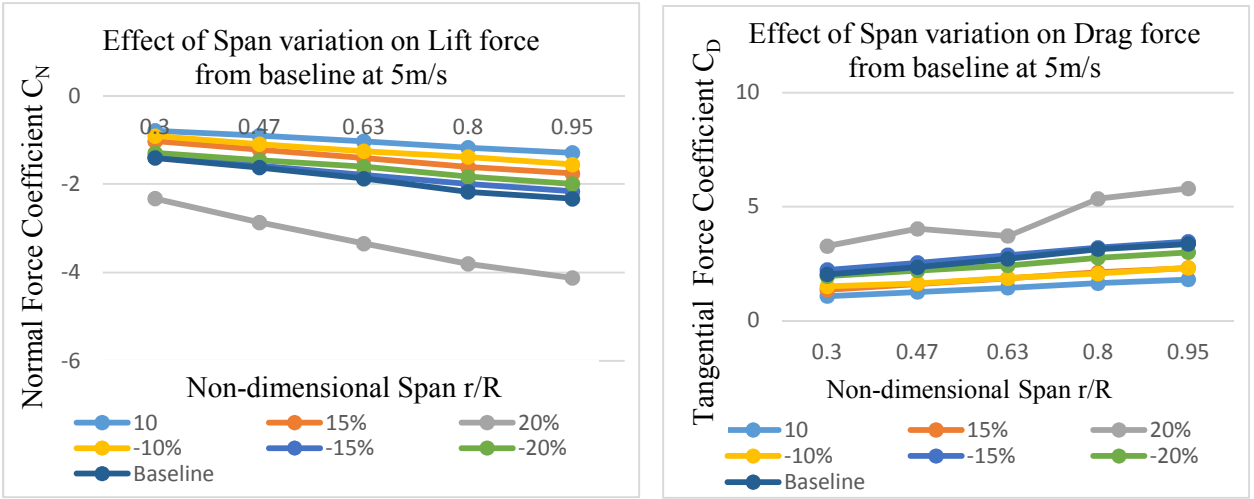

Figure 8: Normal and Tangential force coefficient specification for Span at 5ms^{-1}

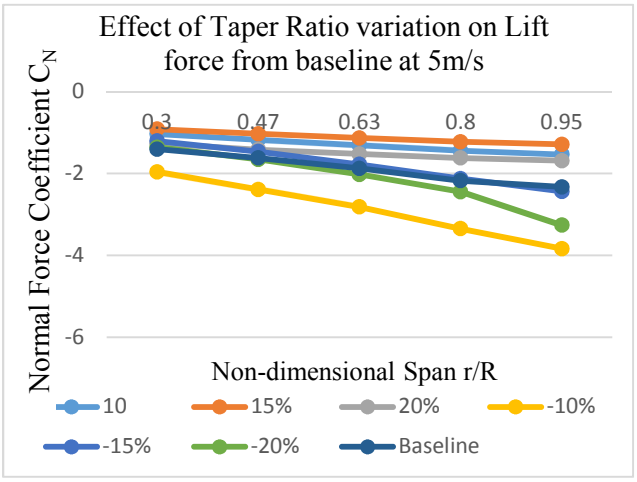

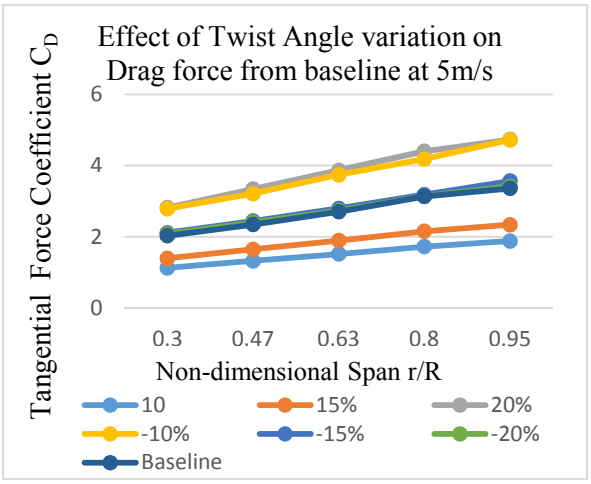

Figure 9: Normal and Tangential force coefficient specification for Taper Ratio at 5ms^{-1}

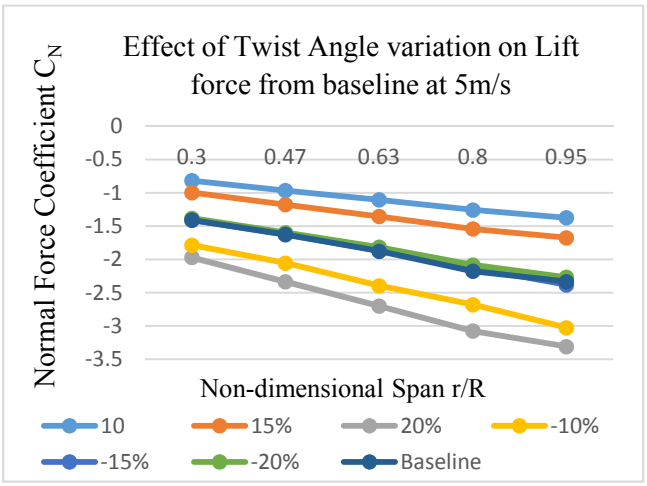

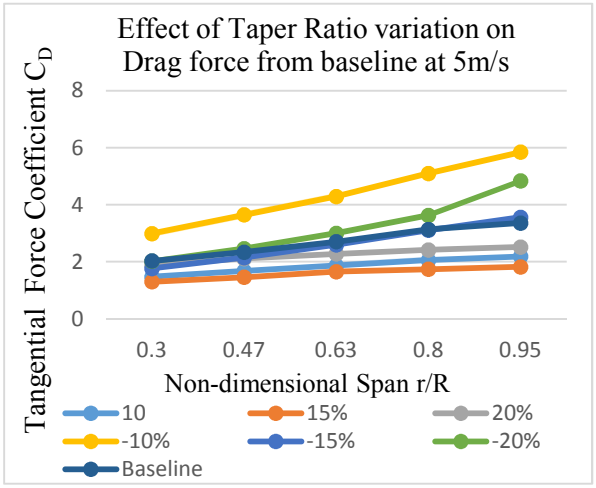

Figure 10: Normal and Tangential force coefficient specification for Twist Angle at 5ms^{-1}.

Two unique experiments are conducted on the 3-D printed blades. The experiments help determine the power output as a function of changes in design parameters. These modifications simulate the real environmental conditions. Experiment 1 involves increasing and decreasing the wind tunnel velocity while keeping the angle of incidence constant. Experiment 2 involves incremental change of angle of incidence while keeping the freestream velocity constant. The Baseline, +20 Twist Angle, and -20% Taper Ratio data results is collected using these experiments to show correlations and discontinuity among the trials. Computational fluid dynamic analysis shows that the +20 twist angle provides the greatest drag force. Yet, it can be expected that the +20% twist angle will generate more power than the -20% taper ratio design. The explanation for this observation is that the twist modification enhances the ability of the blade to maximize initial threshold rotational inertia. This blade model shows promising aerodynamic and structural integrity and durability. If the twist angle is maintained at a correct angle of incidence, the blade will be able to surpass the initial rotational inertia. Physical analysis from wind tunnel experiments shows the corresponding data from each experiment. Figure 11

displays Experiment 1 results. Results show that the -20% taper ratio has the greatest power output slope over the range of wind speeds. The +20 Twist model has a slightly stronger power output than the baseline model.

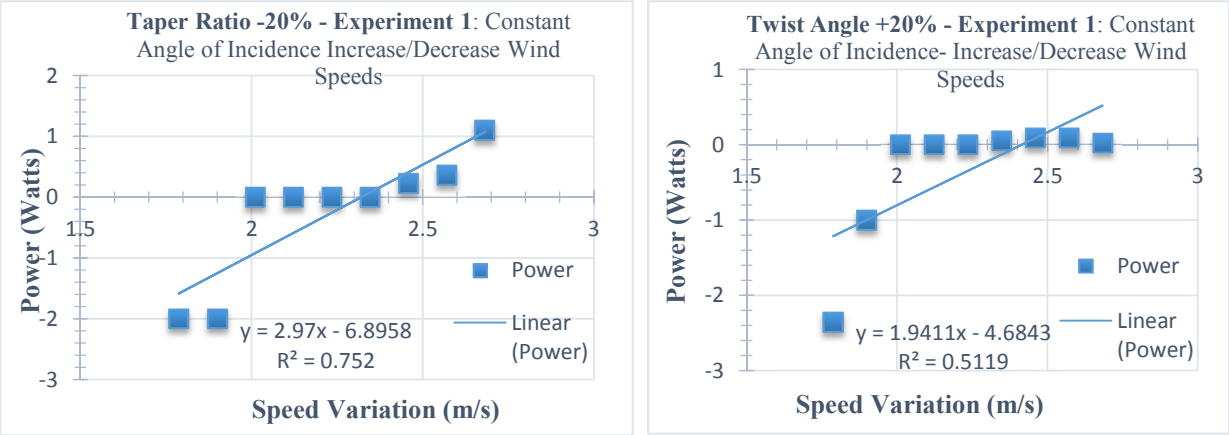

Figure 11: *Experiment 1*- Twist Angle and Taper Ratio constant angle of incidence with speed increase/decrease.

The shallowest slope comes from the baseline model that demonstrates that the modified parameters hold stronger power output than the baseline design. Results of Experiment 2 are shown in Figure 12. The data shows a skewed collection for the Twist Angle variation. The baseline model remains at a constant negative slope as the angle of incidence changes. The maximum power the baseline model delivers is at 48.58 degrees angle of incidence. The reason is that as the pitch angle is increased over a fixed hub, the wind turbine blade essentially reaches a steep angle. The angle will cause the wind blade to act as a drag plate, therefore increasing the drag force, minimizing power output. Possible reasons for variations in power extraction are the limitations of the plastic fabricated blade, gear friction among the rotational turbine gears, skin friction, induced drag etc. The fabrication is a critical variable since the assembly is dependent on the design. The design might have some flaws where air pocket can cause air to seep and form stagnation points within the segmented joints of the turbine blade. This will cause a stagnant pressure to develop in the center of the body not allowing airflow to occur along the z-axis of the blade.

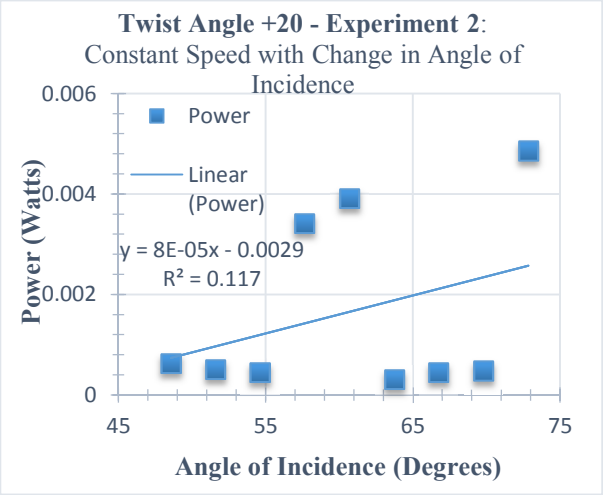

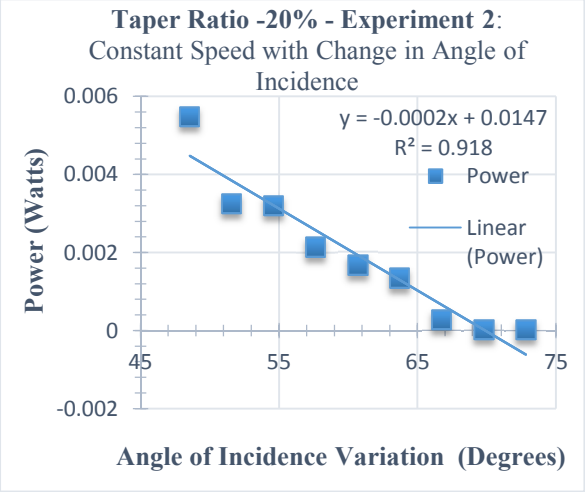

Figure 12: *Experiment 2*- Twist Angle and Taper Ratio constant wind speed with change in angle of incidence.

Results and Discussion

The baseline wind turbine blade is replicated as shown in Figure 13. This design has the first trial assembly design implemented. The 3-D printer is limited to 10in x 10in area. The blade span is greater than that so it would not fit in the available printer area. The blades are split into two halves span wise and these parts are designed and printed separately. Various locking designs are experimented with. The first locking mechanism design uses pins to interconnect the blades together where the pins fit into tolerance slots in the face of the airfoil. Observations from the wind tunnel experimental analysis provide valuable data. Overall, the +20% Taper Ratio has the lowest velocity threshold turn over speed to generate the momentum for the turbine rotation. Since the minimum chord is reduced in size lowering taper ratio, this can lead to lower blade weight. With a light load, the wind turbine blade inertia is reduced. Also there is less surface area to cause drag and skin friction. Once the free stream velocity surpassed the turn over speed, the momentum generated a significant amount of torque resulting in its maximum power output.

For Experiment 1, the +20% Twist Angle and -20% Taper Ratio design resulted in higher power extraction compared to the baseline. The taper ratio reduction displays the greatest output of power overall in Experiment 1. Experiment 2, +20% Twist Angle demonstrates a slightly increasing linear power output as the angle of incidence increases. The reduction in taper ratio shows a negative trend in power extraction. Its highest power extraction is at 48.56 degrees pitch angle. Whereas the twist angle of incidence maximum output power is at72.84 degrees pitch angle. CFD analysis displays similar findings as the experimental wind tunnel test. CFD shows that the increase in twist variations has a slightly higher drag force coefficient than the -20% reduction taper ratio. In wind tunnel testing, this design demonstrates a significant drag force. If not set at its desirable angle of incidence the turbine blade will not initiate rotation.

Figure 13: Baseline pin locking mechanism replica of Wind Turbine Technologies turbine blade

The baseline model is exposed to various experiments to physically test its structural integrity and flexibility. During one of the tests, the baseline turbine blade is destroyed and severed at its joints. Figure 14 shows the aftermath during one of the structural integrity tests. This occurred due to the failure of the adhesive glue and pin joints. The glue that is experimentally in use is a fast plastic glue bond, able to mend the bond among the two joints and inside the slots within several short minutes. After observational analysis, it is concluded that fast glue adhesive is weaker in strength. The bondage does not have enough time to fully mature the and therefore weakens the durability of the ABS Plastic material. The overall pin design is not able to handle the centrifugal forces at its joints. In this design, the pin is the only member holding the wind turbine blades together while rotating at increasing velocities.

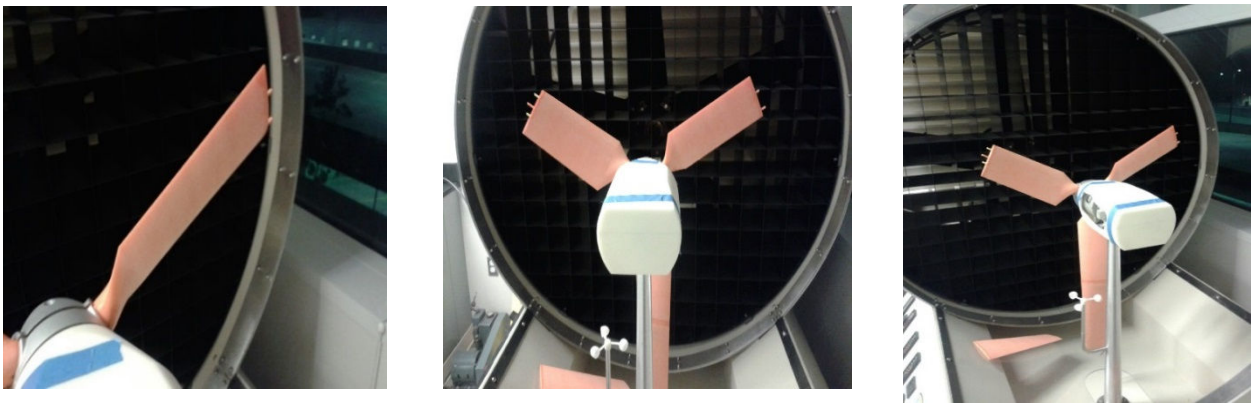

Figure 14: Baseline blade failure of Wind Turbine Technologies model.

A slow bond adhesive is used to join the two parts of the blades together after the failure. Because the bonding takes longer time to set, the joint is more durable. After reconstructing and applying the new slow bond, the baseline blade displays promising durability during wind tunnel testing. The failure of the pin design helps design a new locking mechanism and component. Three particular designs are generated for analysis; key lock, single t-shape lock, and double t-shape lock. The key lock is ruled out because it has too many failure fault points, a similar characteristic to the pin design. The single t-shape lock appeared to have potential, but has a higher possibility of wanting to rotate at its joints. This design will create a moment at its axis due to no other lever arm preventing it from rotating. Figure 15 displays the design locking mechanisms.

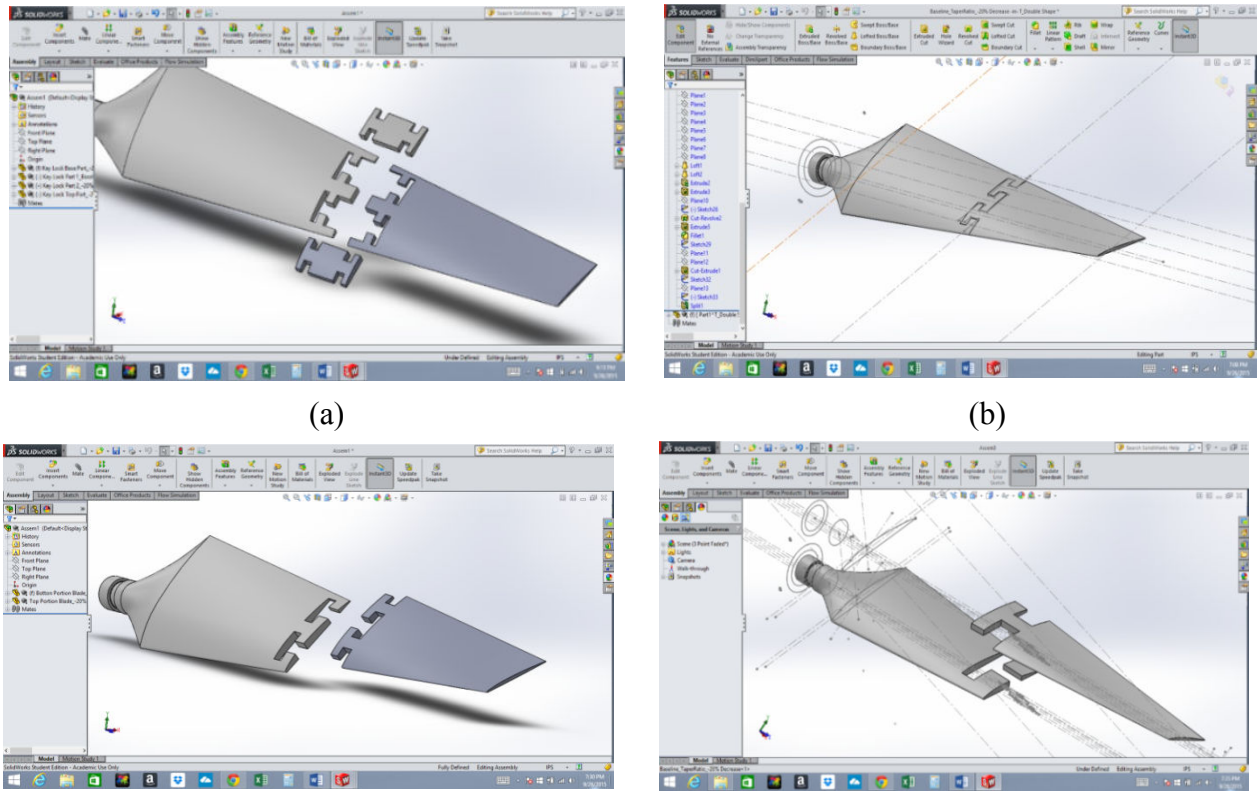

Figure 15: Isometric view of key lock design. (b) Assembled double t-shape lock. (c) Isometric view of double t-lock design. (e) Isometric view of single lock design.

The double t-shape lock is selected to become the new design feature for installments of +20% Twist Angle and -20% Taper Ratio. It is selected because it minimizes the amount of free moving parts used and also prevents moment generated among the joints. This lock displays promising results in maintaining strength from various centrifugal forces, loads, stress, and pressure. Figure 16 shows the complete fabrication of the model turbine blades. The greatest power extraction from the wind tunnel experiments for each design varies. The baseline generated power output from Experiment 1 and 2, 0.000125 Watts at 2.682 m/s, and 0.00075 Watts at 48.56° respectively. The +20% Twist Angle shows 2 x 10-2 Watts for Experiment 1 at 2.682 m/s and 0.00061 Watts in Experiment 2. -20% Taper Ratio in Experiment 1 displays 1.1 Watts at 2.682 m/s, 0.00548 Watts at 48.56° for Experiment 2.

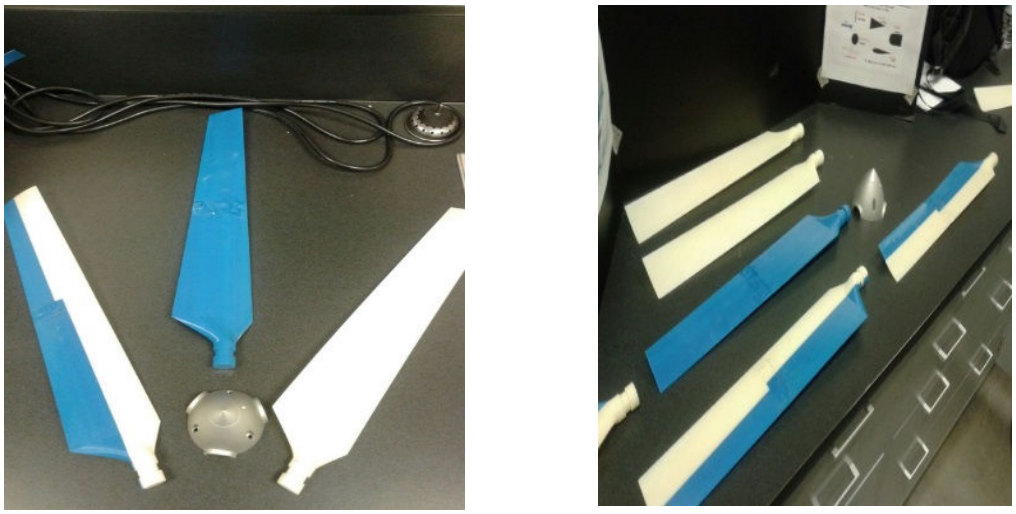

Figure 16: *+20% Twist Angle*: Striped blue and white blade. *-20% Taper Ratio*: Blue blade. *Factory Baseline Blade*: White blade.

The extracted power is compared through wind tunnel experimental testing and numerical calculation for validation studies. The Baseline, +20% Twist Angle, and -20% Taper Ratio blade designs have corresponding power extractions compared to their numerical calculation. The theoretical calculation is measured through total power equation. Total power is the addition of both Induced Power and Profile Power shown in Eq. (3).

$$P_T = Induced\ Power + Profile\ Power \tag{3}$$

Induced Power equation is the product of thrust and induced wind speed, Eq. (4) becomes:

$$P_i = Tv \tag{4}$$

In Eq. (5), the Profile Power is defined as:

$$P_p = \rho A(\Omega R)^3 \frac{\sigma C_{do}}{8}[1 + 3\mu^2] \tag{5}$$

where,

ρ = air density, (kg/m^3)

A = Area of blade profile, (m^2)

$\Omega R = Tip\ Speed$, (m/s)

σ = Solidity Ratio, where ratio of blade area/disk area, (unitless)

C_{do} = Average Drag Coefficient of the Airfoil. $\mu = Advance\ Ratio = \frac{V_\infty}{\Omega R}, where\ V_\infty = Freestream\ Veolcity$, (unitless)

The discrepancy between the power extracted at baseline design and +20 twist angle can be explained by the drag force that causes a large inertia. The -20% taper ratio displays similar trend at initial wind speeds. As the wind speed is increased, the drag force and inertia are overcome, the turbine blades speed up and the power extracted matches the theoretical values more closely. The rotational kinetic energy generates a rapid increase in rotation per minute cycle. It is observed that the minimum speed to cause the turbine blades to start rotating for all three designs are between 2.252 and 2.45872 ms^{-1}. This is also known as turnover speed, the minimum speed for initial rotation. Figures 17 through 19 depict the power extraction analysis comparison for the three blade designs. The figures presents a side by side comparison for precise and accurate representation. Since the experimental value power slope on all three graphs are not increasing as quickly exponentially, each comparison will have an experimental versus theoretical. CFD analysis provides extracted power data at $5ms^{-1}$. This speed is an expected average wind speed on Georgia coastlines, therefore is critical to this study. It can also be noted that performing CFD analysis for each iterative wind tunnel speed and with their corresponding designs can be time consuming. Figure 20 represents the CFD data collection for power results. The CFD analysis leads to the conclusion that the design that extracts the maximum power at $5ms^{-1}$ is the baseline design, followed by +20% twist angle, and -20% taper ratio.

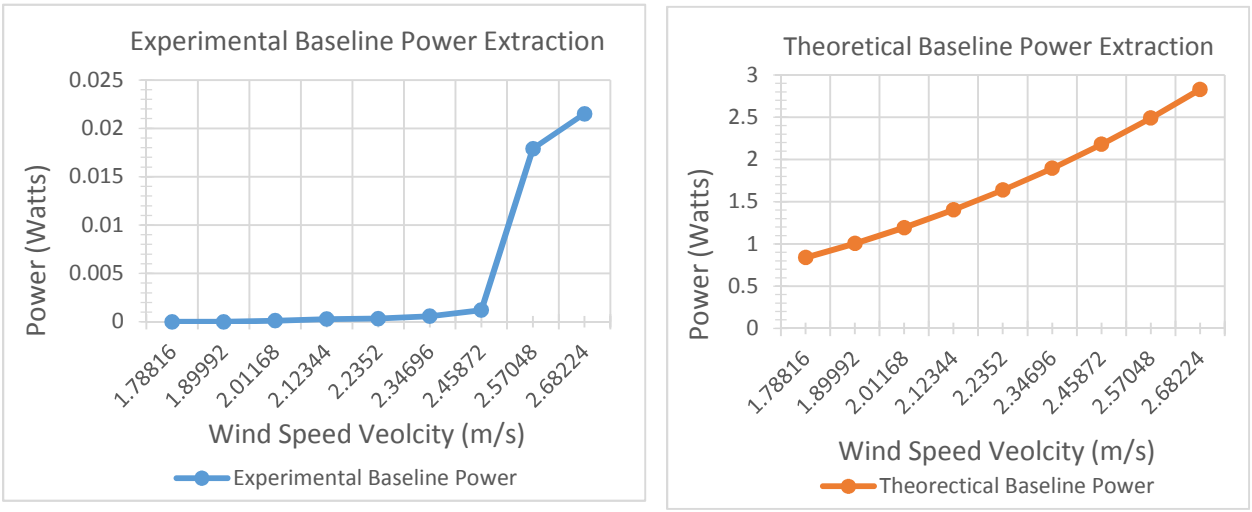

Figure 17: Baseline Power Extraction Comparison.

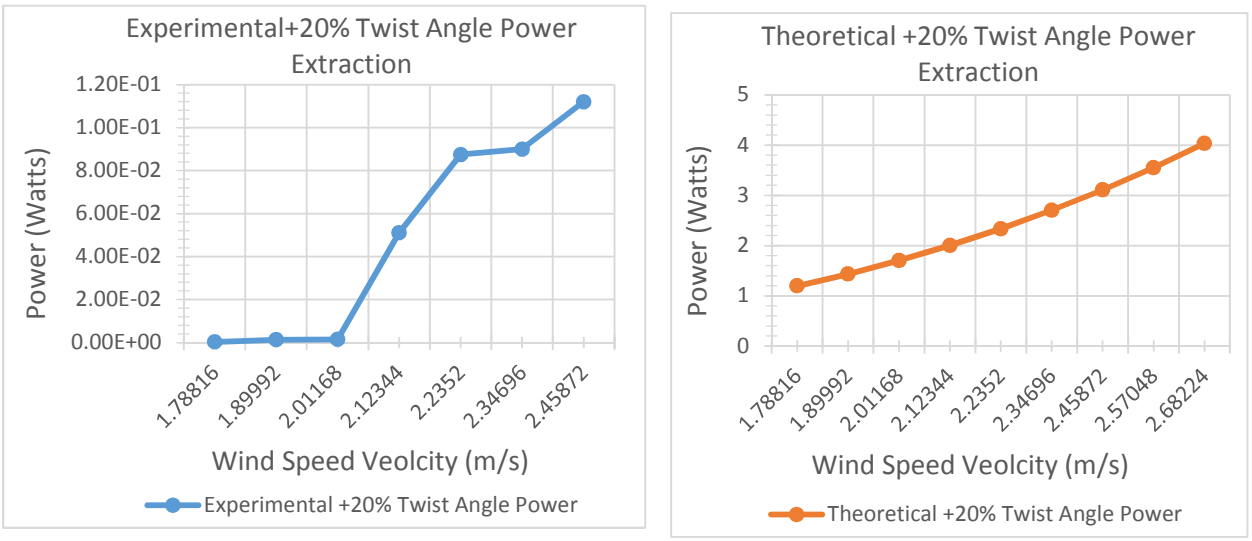

Figure 18: -20% Taper Ratio Power Extraction Comparison.

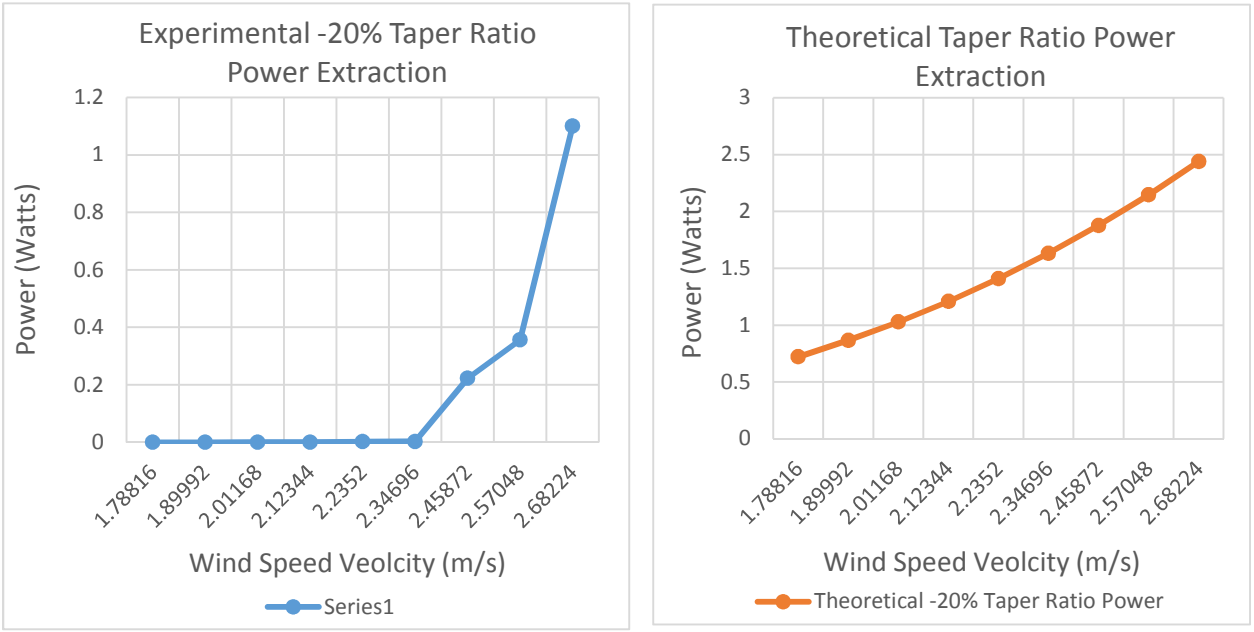

Figure 19: +20% Twist Angle Power Extraction Comparison.

CFD Numerical Power Calculations

	BASELINE	Twist Angle +20	(-) 20 Taper Ratio
Speeds	Power Values (Watts)	Power Values (Watts)	Power Values (Watts)
5 (m/s)	15.45034528	15.05773406	13.81367924

Figure 20: Power Extraction Data from Computational Fluid Dynamic Analysis.

Summary

In summary, the Windlab turbine technologies blade is carefully analyzed, designed, and fabricated to maximize the power extraction from low speed wind occurrences. The application for this experimentation is suitable for small households or low power consumption environments. The approach of theoretical and experimental trials can prove a progression in efficiently maximizing extracted power from wind speeds. Modifications are made to the original turbine technologies blade ranging from increasing or decreasing its physical parameters e.g. maximum chord, span, twist angle, taper ratio, and angle of incidence. Several computer aided design models are created by changing one variable at a time from the baseline blade design. From these model designs, computational fluid analysis is performed in order to determine the best results in terms of maximum lift coefficient, and minimum drag coefficient with respect to it span section. Three computer aided design models are selected for 3D printing physical turbine blades. From the data collection, the best CFD results are obtained for the 20% increase in twist and -20% reduction in taper ratio. The -20% taper ratio displays the highest lift coefficient, versus the +20% in twist, that results in slightly higher drag coefficient. With a theoretical prediction based of CFD analysis, the most promising blade model turns out to be the +20% Taper Ratio. In wind tunnel analysis, the taper ratio design provides the maximum extraction of power over any other 3-D printed designs at 48.56° with 2.682 m/s wind speed.

Through extensive experimentation, the physical 3D printed models are then compared to their counterparts from CFD analysis in terms of most power extracted per revolutions per minute. This provides promising results for researching and exploring designs to extract maximum power for low speed winds. Two laboratory experiments are implemented to test the printed and fabricated blade models. Experiment 1 consists of maintaining constant angle of incidence with decreasing and gradually increasing wind speed. Experiment 2 involves constant wind velocity with change in angle of incidence from 48.56 ° to 72.84° respectively. The results from CFD analysis correlate with the wind tunnel testing of the +20 increase taper ratio; it displays the highest extracted power slope. CFD analysis results display that the +20 Twist Angle has a higher drag coefficient. The laboratory tests show that the +20% twist results in more drag during pitch changes. Observation shows that it took more wind speed to generate initial rotation; this is due to the significant drag force from the twist opposing the rotation. The slope is slightly steeper than the maximum taper ratio design. Therefore both designs in Experiment 2 show similar characteristics in power output. These values show a small slope with little output due to the lack of turn over speed. Each wind turbine has a unique property and characteristics to overcome the inertia for rotation.

Theoretically, if the wind speed for Experiment 2 is increased; the power output values will show promising results. This experimentation is a foundation to explore future work with many additional aerodynamic design parameters to be explored. These include changing the type of airfoil used, modifying blade span, maximum chord, etc. In further analysis, this experiment will obtain power output values displayed from each turbine blade design and equate them within a power equation to provide accurate results. Possible cross over points in design for future modifications may be studied to model best results.

The power extraction analysis shows a comparison of theoretical versus numerical experiment. The correlation of all the plot slopes shows an incremental increase in power as speed is

increases. Each three blade designs show their respective characteristics when exposed to external wind speeds. From the power extraction comparison analysis, the -20% Taper Ratio plot displays are higher power observation. CFD analysis provides data that the baseline design surpasses its processors and contradicts the power extraction comparisons.

Conclusion

The present study allows an undergraduate student to go through a complete engineering design cycle. They start with a baseline wind turbine and calculate the lift and drag using analytical methods. The values are then compared with a corresponding wind turbine blades designed using CAD. Validation is performed to ensure that the CFD software is calibrated. Various wind turbine parameters are changed and power extracted values are calculated. This activity allows the undergraduate student to experience a complete engineering research process. The undergraduate student has indicated that as a result of this work, their confidence in pursuing engineering studies and research has increased; they are now interested in pursuing graduate work and hope to continue to do more of the same or similar work into the future. It is expected that as part of this study the student will continue to work on the project and look at the effects of varying the blade aspect ratio, chord, type of airfoil and taper on the turbine efficiency. Possibly future explorations include conducting the Computational Fluid Dynamic analysis testing at the same low wind tunnel speeds for stronger data analysis.

References

1 Chiang, E. P., Zainal, Z. A., Narayana, P. A., and Seetharamu, K. N. (2000). Potential Of renewable wave and offshore wind energy sources in Malaysia.

2 Din, Abdul Talib, Shamsul Bahari Azraai, and Kesavan Thenamirtham. Design and Development of a Vertical Wind Turbine Using Slow Wind Speed for Mini Power Generation. Tech. N.p.: Elsevier, 2008. Future Energy Journal for Our Planet.

3 Elfarral, Monier A., Nilay Sezer Uzol, and Sinan Akmandor NREL VI Rotor Blade: Numerical Investiagion and Winglet Design and Optimization Using CFD. Tech Journal of Fluids Engineering 2002; 124: 393-399.

4 "Wind Turbine Power System." Turbine Technologies, n.d. Web. 31 July 2015.

5 “Georgia Wind Resource Map and Potential Wind Capacity. “ WIND Exchange; U.S. Department of Energy, n.d Web. 26 July 26, 2015

6 “Wind Map | NOAA Climate.gov.” Wind Map | NOAA Climate.gov. National Centers for Environmental Information, n.d, Web. 25 July 2015.

7 "Renewable & alternative fuels." Electric Power Annual, 23 Mar. 2015. Web

8 Smith, J., A. Huskey, D. Jager, and J. Hur. "Wind Turbine Generator System Safety and Function Test Report for the Entegrity EW50 Wind Turbine." Wind Turbine Generator System Safety and Function Test Report for the Entegrity EW50 Wind Turbine (2012): n. pag. National Renewable Energy Laboratory. Web. 2015.

9 Satpathy, A.S.; Kishore, N.K.; Kastha, D.; Sahoo, N.C. "Control Scheme for a Stand-Alone Wind Energy Conversion System", Energy Conversion, IEEE Transactions on, On page(s): 418 - 425 Volume: 29, Issue: 2, June 2014

10 R. D. Richardson and G. M. Mcnerney "Wind energy systems", Proc. IEEE, vol. 81, no. 3, pp.378 -389 1993

11 A. D. Sahin "Progress and recent trends in wind energy", Progress in Energy Combustion Sci., vol. 30, no. 5, pp.501 -543 2004

12 A. Chakraborty "Advancements in power electronics and drives in interface with growing renewable energy resources", Renewable Sustainable Energy Rev., vol. 15, no. 4, pp.1816 -1827 2011

13 A. M. D. Broe, S. Drouilhet and V. Gevorgian “A peak power tracker for small wind turbines in battery charging applications", IEEE Trans. Energy Convers., vol. 14, no. 4, pp.1630 -1635 1999

14 Robert Howell, Ning Qin, Jonathan Edwards, Naveed Durrani, ‘Wind tunnel and numerical study of a small vertical axis wind turbine,’ Renewable Energy, Volume 35, Issue 2, February 2010, Pages 412–422

15 Abdullah Mobin Chowdhurya, Hiromichi Akimotoa, Yutaka Harab, ‘Comparative CFD analysis of Vertical Axis Wind Turbine in upright and tilted configuration,’ Renewable Energy, Volume 85, January 2016, Pages 327–337

16 Alessandro Bianchini, Francesco Balduzzi, John M. Rainbird, Joaquim Peiro, J. Michael R. Graham, Giovanni Ferrara and Lorenzo Ferrari, ‘An Experimental and Numerical Assessment of Airfoil Polars for Use in Darrieus Wind Turbines—Part I: Flow Curvature Effects,’ J. Eng. Gas Turbines Power 138(3), 032602, Sep 22, 2015

17 Francesco Balduzzia, Alessandro Bianchinia, Riccardo Malecia, Giovanni Ferraraa, Lorenzo Ferrarib, ‘Critical issues in the CFD simulation of Darrieus wind turbines,’ Renewable Energy, Volume 85, January 2016, Pages 419–435

18 Van Treuren, K.W., ‘Small-scale wind turbine testing in wind tunnels under low Reynolds number conditions,’ 2015 Journal of Energy Resources Technology, Transactions of the ASME

19 Emejeamara, F.C., Tomlin, A.S., Millward-Hopkins, J.T., ‘Urban wind: Characterization of useful gust and energy capture,’ 2015 Renewable Energy

20 Dossena, V., Persico, G., Paradiso, B., Brighenti, A., Benini, E., ‘An experimental study of the aerodynamics and performance of a vertical axis wind turbine in a confined and unconfined environment,’ 2015 Journal of Energy Resources Technology, Transactions of the ASME